Phase control of nonlinear Breit-Wheeler pair creation

B. Barbosa* and M. Vranic
GoLP/Instituto de Plasmas e Fusão Nuclear, Universidade de Lisboa, 1049–001 Lisbon, Portugal

K. Weichman, D. Ramsey, and J. P. Palastro
Laboratory for Laser Energetics, University of Rochester, Rochester, New York 14623, USA

(Received 29 October 2023; accepted 1 April 2024; published 10 May 2024)

Electron-positron pair creation occurs throughout the universe in the environments of extreme astrophysical objects, such as pulsar magnetospheres and black hole accretion disks. The difficulty of emulating these environments in the laboratory has motivated the use of ultrahigh-intensity laser pulses for pair creation. Here we show that the phase offset between a laser pulse and its second harmonic can be used to control the relative transverse motion of electrons and positrons created in the nonlinear Breit-Wheeler process. Analytic theory and particle-in-cell simulations of a head-on collision between a two-color laser pulse and electron beam predict that with an appropriate phase offset, the electrons will drift in one direction and the positrons in the other. The resulting current may provide a collective signature of nonlinear Breit-Wheeler, while the spatial separation resulting from the relative motion may facilitate isolation of positrons for subsequent applications or detection.

DOI: 10.1103/PhysRevResearch.6.023152

I. INTRODUCTION

The environment of extreme astrophysical objects feature electromagnetic fields with sufficient strength to convert photons into electron-positron pairs [1–12]. The large-scale production of pairs forms a dense pair plasma that plays a critical role in the dynamics of the environment. While observable signals from the pair plasma, such as γ-ray bursts [13–17], provide valuable insights into these dynamics, the complex interplay of physical processes within the environment make it difficult to study any single phenomenon in isolation. Focused simulation and laboratory studies can help build connections between the microscale processes and macroscale dynamics. For instance, the currents generated during lepton creation and motion can seed filamentation-type instabilities [18–21] or field generation mechanisms, such as Biermann battery [22], that modify the macroscopic behavior. By emulating the conditions of extreme astrophysical objects, laboratory experiments can also isolate phenomena and validate the simulation tools used for their study. Relativistic particle beams and ultrahigh-intensity laser-matter interactions offer two approaches to these experiments [23–26].

The strong-field quantum electrodynamical (QED) processes responsible for pair creation are at the current frontier of high-intensity laser-matter interactions [27–35]. Creative configurations for these interactions allow for pair production at field strengths well below the characteristic electric (magnetic) field of nonlinear QED, i.e., the Sauter-Schwinger field equal to $10^{18}\,\mathrm{V/m}$ ($10^{9}\,\mathrm{T}$) [36,37]. For instance, irradiating a thin, high-atomic number target with an intense laser pulse can energize a population of electrons. The bremsstrahlung photons emitted by the electrons subsequently decay into pairs through the Bethe-Heitler process [29,30,38]. As another example, the combined fields of a plasma and laser pulse channeling through a thin, dense target can rapidly accelerate electrons, resulting in both forward and backward photon emission. The collision of the counter-propagating photons can produce pairs through the linear Breit-Wheeler process [39,40].

The nonlinear Breit-Wheeler process can be used to generate pairs without a dense target in near-vacuum conditions. In a typical configuration, an ultrahigh-intensity laser pulse collides head on with relativistic electrons [27]. Nonlinear Compton scattering (NCS) of low-energy optical photons from the electrons produces high-energy photons. Immersion of the high-energy photons in the fields of the intense laser pulse allows for their decay into electron-positron pairs, i.e., Breit-Wheeler pair creation. Under the right conditions, subsequent NCS from the pairs can ignite a QED cascade, where the number of leptons grows exponentially—the ultimate result of which is a pair plasma [28,41–53].

Regardless of the scheme used for pair creation, several effects can challenge reliable diagnosis and analysis of experimental results. These include direct trident pair creation [54] or bremsstrahlung and Bethe-Heitler byproducts from the unintended interaction of the laser pulse or charged particles with experimental equipment. Methods for separating the electrons from the positrons in a predictable way can facilitate detection and diagnosis of the pairs. Conventionally, this is done by deflecting both species in a static magnetic field (on

*bernardo.barbosa@tecnico.ulisboa.pt

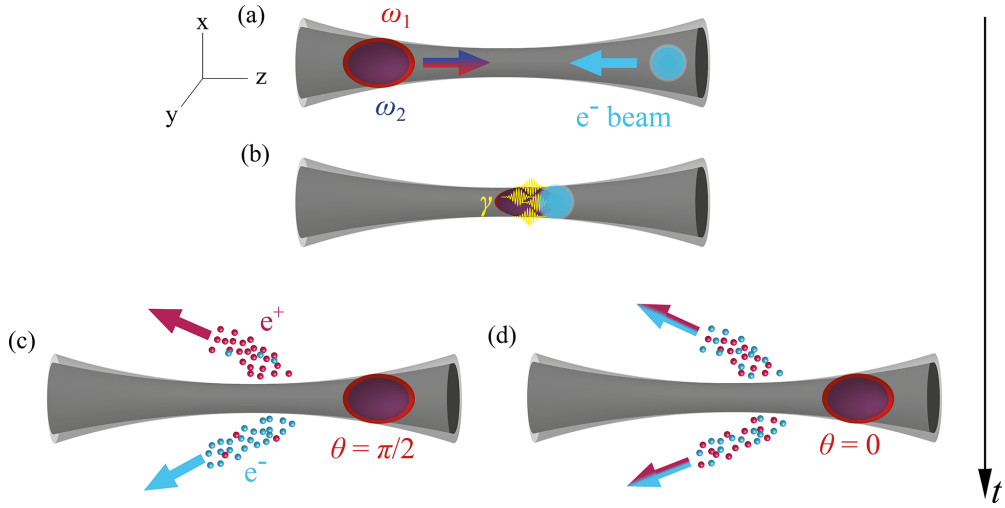

FIG. 1. Schematic of the electron beam-laser pulse interaction for controlling the relative motion of electrons and positrons created by the nonlinear Breit-Wheeler process. (a) The electron beam and two-color laser pulse right before their head-on collision. The harmonics composing the laser pulse have the same focused spot size and focal plane. The transverse width of each harmonic along its propagation path is displayed in gray. (b) Nonlinear Compton scattering during the collision of the electrons and laser pulse produces hard photons (γ rays) shown in yellow. The interaction of the hard photons with the laser pulse produces electron-positron pairs. (c) For a phase offset between the harmonics $\theta = \pi/2$, the electrons and positrons drift in opposite directions. (d) For a phase offset $\theta = 0$, the electrons and positrons drift in both directions.

the order of 1 T) [27,29,30]. However, this technique separates the pairs far from the interaction region. As an alternative, the field of an ultrahigh-intensity laser pulse can be structured to deflect the electrons and positrons in opposite directions at the instant of their creation.

Here we demonstrate that the relative transverse motion of electrons and positrons created in the nonlinear Breit-Wheeler process can be controlled using a laser pulse composed of a fundamental and an appropriately phased second harmonic. By adjusting the relative phase of the harmonics, the electrons can be made to drift in one direction and the positrons in the other (Fig. 1). The presence of the second harmonic (or any even harmonic) breaks the symmetry of the field and allows the charges to drift in opposite directions. This cannot be achieved using odd harmonics alone. The two-color field configuration is motivated by techniques for coherent control used in photoionization, photoemission, molecular orientation, radiation reaction, and electron-positron spin polarization [55–62] .

The remainder of this manuscript is organized as follows. Section II describes the pair-creation scheme and presents an analytical model for the pair motion and current. Comparisons with 1D QED-particle-in-cell (QED-PIC) simulations [63–66] of a two-color laser pulse colliding with hard photons show that the model successfully predicts the scaling of the pair current with the relative phase and amplitude of the harmonics. Section III presents full-scale, 2D QED-PIC simulations of a focused laser pulse colliding with a relativistic electron beam for parameters relevant to near-term, high-power laser facilities. Despite the ponderomotive force of the focused pulse, the relative phase of the harmonics still provides control over the relative transverse motion of the created electrons and positrons. Section IV summarizes the results and discusses future prospects.

II. PAIR CREATION IN TWO-COLOR LASER PULSES

Figure 1 illustrates the configuration for pair creation. A relativistic electron beam (blue) collides head on with a laser pulse composed of a first and second harmonic (red and dark blue ellipsoids) [Fig. 1(a)]. Rapid acceleration of the electrons in the fields of the laser pulse results in the emission of hard photons (γ rays) through nonlinear Compton scattering [Fig. 1(b)]. These photons counterpropagate with respect to the laser pulse, simultaneously interact with multiple optical photons, and decay into pairs through the nonlinear Breit-Wheeler process [Figs. 1(c) and 1(d)].

The pair creation rate and subsequent particle dynamics depend on the phase of the optical field at the instant of creation and the phase offset θ between the two harmonics. The phase at the instant of creation determines the local field strength, while the phase offset determines the shape of the optical waveform. Tuning the phase offset to structure the optical waveform provides control over the relative transverse motion of the created electrons and positrons [Figs. 1(c) and 1(d)].

The relative motion of the electrons and positrons can be described by an analytical model for the evolution of the pairs in the electromagnetic fields of the laser pulse. The laser pulse propagates in the positive $\hat{\mathbf{z}}$ direction and is polarized in the $\hat{\mathbf{x}}$ direction. The normalized four-potential $\mathcal{A}^\mu = eA^\mu/mc$ of the pulse is modeled as a plane wave

$$\mathcal{A}^\mu = [\mathrm{a}_1(\phi)\sin(\phi) + \mathrm{a}_2(\phi)\sin(2\phi+\theta)]\epsilon^\mu = a(\phi)\epsilon^\mu, \tag{1}$$

where c is the vacuum speed of light, e and m are the charge and mass of a positron, $\phi = k^\mu x_\mu = t - z$ is the phase variable with $x^\mu = (t, x, y, z)$ and $k^\mu = (1, 0, 0, 1)$, and $\epsilon^\mu = (0, 1, 0, 0)$ is the polarization four vector. The envelopes a_1 and a_2 describe the temporal profiles of the first and second

harmonic with maximum values a_1 and a_2. Here and throughout, time and space are normalized to $1/\omega_1$ and c/ω_1, where ω_1 is the angular frequency of the first harmonic.

After creation, the electrons and positrons evolve according to the relativistic equation of motion including the Landau-Lifshitz model for radiation reaction [67]

$$\frac{dp^\mu}{d\tau} = \pm F^{\mu\nu}p_\nu \pm \frac{2}{3}r_e(\partial_\nu F^{\mu\rho})p^\nu p_\rho - \frac{2}{3}r_e F^{\mu\nu}F_{\rho\nu}p^\rho + \frac{2}{3}r_e(F^{\nu\rho}p_\rho)^2 p^\mu, \tag{2}$$

where τ is the proper time, $p^\mu = (\gamma, p_x, p_y, p_z)$ is the momentum four vector normalized to mc, $\gamma = (1 + |\mathbf{p}|^2)^{1/2}$, $F^{\mu\nu} = \partial^\mu \mathcal{A}^\nu - \partial^\nu \mathcal{A}^\mu$ is the electromagnetic tensor, and r_e is the classical electron radius. The upper and lower signs are taken for electrons and positrons, respectively. For a four potential that depends solely on the coordinates in the combination $\phi = t - z$ [as in Eq. (1)], the equation of motion can be solved analytically [68]. The solution is

$$p^\mu = \frac{1}{h(\phi,\phi_0)}\left\{p_0^\mu \pm \frac{1}{\rho_0}I(\phi,\phi_0)f^{\mu\nu}p_{0,\nu} + \frac{1}{2\rho_0}[h^2(\phi,\phi_0) - 1 + I^2(\phi,\phi_0)]k^\mu\right\}, \tag{3}$$

where p_0^μ is the momentum four vector at the moment the particle is created, $\rho_0 = p_0^\mu k_\mu$, $f^{\mu\nu} = k^\mu \epsilon^\nu - k^\nu \epsilon^\mu$,

$$h(\phi,\phi_0) = 1 + \frac{2}{3}r_e\rho_0\int_{\phi_0}^{\phi}[a'(\varphi)]^2 d\varphi,$$

$$I(\phi,\phi_0) = \int_{\phi_0}^{\phi}[h(\varphi,\phi_0)a'(\varphi) + (2/3)r_e\rho_0 a''(\varphi)]d\varphi,$$

ϕ_0 is the phase at the time of creation, and $'$ denotes a derivative with respect to the argument.

Using Eq. (3), one can show that the created particles move in the polarization direction with a velocity ($\boldsymbol{\beta} = \mathbf{p}/\gamma$) given by

$$\beta_x(\phi,\phi_0) = \frac{2(\gamma_0 - p_{z0})[p_{x0} \mp I(\phi,\phi_0)]}{h^2(\phi,\phi_0) + (\gamma_0 - p_{z0})^2 + [p_{x0} \mp I(\phi,\phi_0)]^2 + p_{y0}^2}. \tag{4}$$

Because the laser pulse has a finite duration, the particles will eventually leave the vicinity of the pulse. As they do so, their transverse velocity asymptotes to $\beta_{xf}(\phi_0) \equiv \beta_x(\phi_0, \phi \to \infty)$. In the absence of radiation reaction, this simplifies to

$$\beta_{xf}^{\text{class}}(\phi_0) = \frac{2(\gamma_0 - p_{z0})[p_{x0} \pm a(\phi_0)]}{1 + (\gamma_0 - p_{z0})^2 + [p_{x0} \pm a(\phi_0)]^2 + p_{y0}^2}. \tag{5}$$

Equations (4) and (5) demonstrate that after interacting with the laser pulse, the particles drift in the transverse direction with a velocity determined by their charge and the phases of the harmonics at the time of their creation, ϕ_0 and $2\phi_0 + \theta$ [Figs. 2(e)–2(f)].

The initial momenta of an electron-positron pair are determined by the energy and momentum of the hard photon responsible for their creation. In the configuration of interest here (Fig. 1), the incident electron beam is composed of ultrarelativistic electrons with $-p_z \approx \gamma \gg |\mathbf{a}|$. As a result, the hard photons produced by NCS travel predominantly in the negative $\hat{\mathbf{z}}$ direction with $k^\mu \approx (\omega, 0, 0, -\omega)$, where ω is the angular frequency of the hard photon. When a photon decays, its momentum and energy are divided between the resulting electron (e) and positron (p), such that $p_{x0} \approx 0$ and $\gamma_0^e + \gamma_0^p = \omega/a_s$, where $a_s = m_e c^2/\hbar\omega_1$ is the normalized vector potential corresponding to the Schwinger field [65,69,70].

The partitioning of the hard photon energy between the electron and positron is determined probabilistically by the differential rate for nonlinear Breit-Wheeler pair creation $d^2N_{BW}/dtd\eta$ [71–73], where $\eta = |(F_{\mu\nu}p^\mu)^2|^{1/2}/a_s$ is the Lorentz-invariant quantum nonlinearity parameter. At the instant of creation,

$$\eta(\gamma_0,\phi_0) = 2\gamma_0\frac{|a_1(\phi_0)\cos(\phi_0) + 2a_2(\phi_0)\cos(2\phi_0+\theta)|}{a_s}. \tag{6}$$

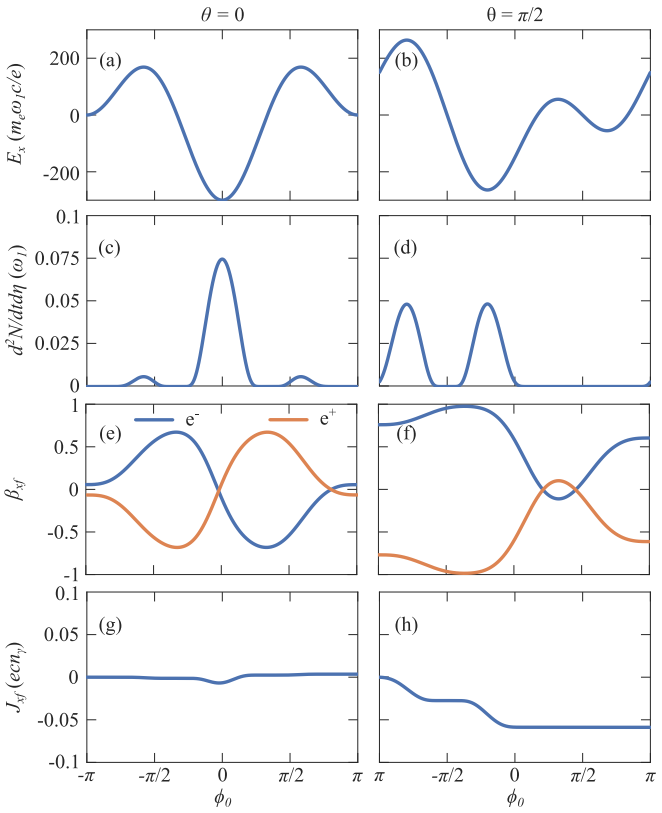

FIG. 2. (a), (b) The total electric field of the two-color laser pulse; (c), (d) differential pair creation rate; (e), (f) asymptotic drift velocity β_{xf} (for created positrons in orange and electrons in blue); and (g), (h) cumulative, asymptotic transverse current density of the created pairs for a relative phase of $\theta = 0$ (left) and $\theta = \pi/2$ (right). The laser pulse is comprised of a fundamental and second harmonic with wavelengths $\lambda_1 = 2\pi c/\omega_1 = 1\,\mu\text{m}$ and $\lambda_2 = 0.5\,\mu\text{m}$ and amplitudes $a_1 = 150$ and $a_2 = 75$. The incident hard photon had $\hbar\omega/m_e c^2 = 500$, and its energy was divided evenly between the created electron and positron. When $\theta = \pi/2$, the asymmetric drift velocity and pair creation rate result in the accumulation of a transverse current.

The differential rate is a sensitive function of η, and thus of the phases ϕ_0 and θ.

Figures 2(a)–2(f) illustrate the dependence of the differential pair creation rate $dN_{BW}/dtd\eta$ and the asymptotic drift velocity β_{xf} on ϕ_0 and θ. The maxima of the rate coincide with extrema of the electric field, $\mathbf{E} = -\partial_t \boldsymbol{\mathcal{A}}$. When $\theta = 0$, the drift is nearly antisymmetric about the peak of the rate [Figs. 2(c) and 2(e)], resulting in minimal current [Fig. 2(g)]. When $\theta = \pi/2$, the drift has the same sign for all phases in which pairs are born [Figs. 2(d) and 2(f)], resulting in a substantial electron-positron current [Fig. 2(h)].

For a monoenergetic beam of hard photons, the asymptotic transverse current density of created pairs is given by

$$J_{xf} = 2e \iint_{\eta_{\min}}^{\eta_{\max}} \beta_{xf} \frac{d^2N_{BW}}{dtd\eta} n_\gamma d\eta d(\phi_0/2), \tag{7}$$

where n_γ is the number density of photons, $\eta_{\min} = \eta(1, \phi_0)$, and $\eta_{\max} = \eta(\omega/a_s - 1, \phi_0)$. The factor of 2 accounts for the equal contribution to the current from positrons and electrons, while the factor of $1/2$ accounts for counterpropagation of the hard photons with respect to the laser pulse. Figures 2(g) and 2(h) show the cumulative integral of the current density over a single phase of a two-color laser field.

A phase offset of $\theta = \pi/2$ produces the largest relative drift between the created electrons and positrons and maximizes the transverse current density [Fig. 3(a)]. This prediction of the analytical model agrees with 1D QED-PIC simulations of planar laser pulses colliding head on with monoenergetic, hard-photon beams (see the Appendix for details). Both the model and simulations also predict that the current density is maximized for $a_1 \approx 160$ and $a_2 \approx 70$ when the total energy (fluence in 1D) of the laser pulse is held fixed [Fig. 3(b)]. This maximum is the result of two effects. First, in the limit that either harmonic has all of the energy, the asymmetry in the field is eliminated, and there is no asymptotic transverse current [$a_1 = 0$ and 210 in Fig. 3(b)]. Second, the maximum electric field of the total waveform, and thus the maximum creation rate, occurs when the electric field strengths of the harmonics are equal ($a_1 \approx 150$ in Fig. 3).

The differential pair creation rate and asymptotic current increase nonlinearly with the energy of the hard photons up to a value of $\chi \gtrsim 1$, where $\chi = 2\omega|\mathbf{E}|/a_s^2$ is the Lorentz-invariant quantum nonlinearity parameter of the photons. When the photon energy is large enough ($\chi \sim 1$), prolific creation of pairs significantly depletes the number of available photons. More specifically, the photon number density evolves according to

$$n_\gamma(\phi_0) = n_{\gamma i} \exp\left[-\int_{-\infty}^{\phi_0} \int_{\eta_{\min}}^{\eta_{\max}} \frac{d^2N_{BW}}{dtd\eta} d\eta d(\phi_0/2)\right], \tag{8}$$

where $n_{\gamma i}$ is the density of the incident photon beam. For Fig. 3, this correction to the photon density was applied in Eq. (7), resulting in excellent agreement between the theory and simulations.

III. PHASE CONTROL WITH FOCUSED LASER PULSES

The model and simulations presented in the previous section illustrated the salient phenomena that allow for phase control of nonlinear Breit-Wheeler pair creation. Several effects, however, were not considered: the generation of nonmonoenergetic photons from NCS, quantum radiation reaction, and the transverse ponderomotive force of the laser pulse. This section presents full-scale 2D QED-PIC simulations that include these effects and verify that the underlying physical picture remains unchanged.

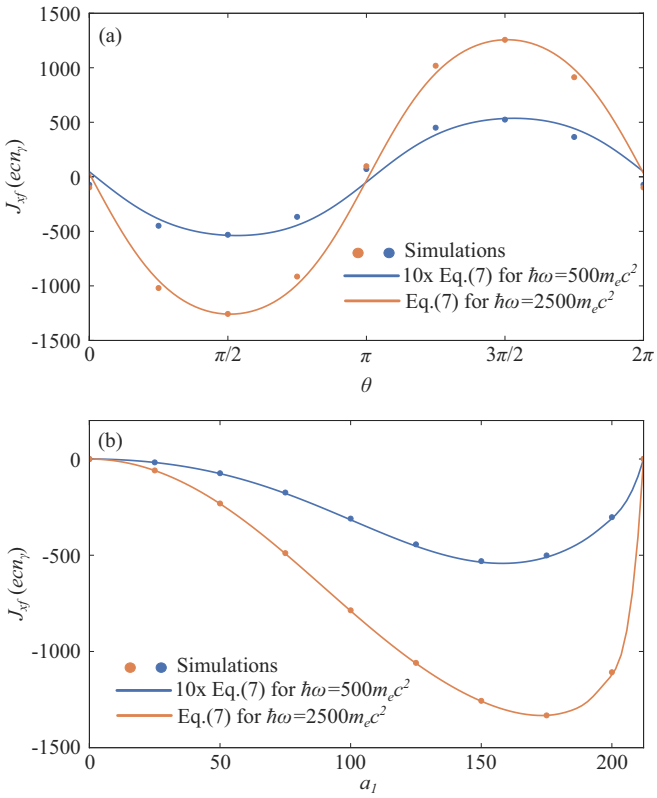

FIG. 3. Comparison of the asymptotic transverse current density predicted by the analytical theory (continuous curves) and 1D simulations (dots) as a function of (a) the phase offset between the first and second harmonic of the laser pulse θ and (b) the amplitude of the first harmonic a_1 for a fixed fluence of 1.4×10^9 J/cm^2 and a full-width-half-maximum duration of 23 fs. In (a) $a_1 = 150$, while in (b) $\theta = \pi/2$. The currents for the photon energy $\hbar\omega = 500m_ec^2$ where multiplied by ten to make them visible on the same scale as the $\hbar\omega = 2500m_ec^2$ currents. The theory [Eq. (7)] and simulations are in excellent agreement.

In 2D (or 3D), the relative drift of the electrons and positrons eventually results in their spatial separation, which can facilitate experimental detection and diagnosis. To illustrate the spatial separation and demonstrate phase control for realistic, focused laser pulses, the head-on collision of a two-color laser pulse and a relativistic electron beam was simulated using 2D QED-PIC (see the Appendix for details). The laser pulse and electron beam parameters are motivated by near-term high-intensity laser facilities and current laser wakefield accelerators, respectively. The parameters are displayed in Table I [74–81]. The simulated interaction was synchronized so that the peak intensity of the laser pulse and the peak density of the electron beam arrived at the focal plane ($z = 0$) at the same time. Note that the number of photons

TABLE I. Parameters for the 2D QED-PIC simulations. Where applicable, the parameters are the same as in the 1D simulations presented in Sec. II. The electron beam had a Gaussian profile in all directions, while the laser pulse had a Gaussian profile in the transverse direction and a polynomial profile in the longitudinal direction (see the Appendix). The focal spot, length, and width are specified as the e^{-2} values.

Laser pulse parameters	Value
λ_1 (μm)	1
λ_2 (μm)	0.5
a_1	150
a_2	75
λ_1 & λ_2 FWHM duration (fs)	23
λ_1 & λ_2 focal spot (μm)	6
Total Energy (J)	800
Electron beam parameters	**Value**
Length (μm)	6
Width (μm)	6
Charge (pC)	10
Energy (GeV)	5.1

generated in NCS, and hence the number of pairs, is linearly proportional to the number of beam electrons. Thus, the pair and current densities can be linearly scaled to obtain the result for higher or lower beam charges.

Figure 4 displays the charge densities and momentum distributions of the created electrons and positrons ∼65 fs after the initial collision of the laser pulse and the electron beam. A phase offset of $\theta = \pi/2$ maximizes the relative drift (transverse momenta) and spatial separation of the electrons and positrons: The electrons travel predominantly in the positive x direction and the positrons in the negative x direction. As the charges advance into the "far field," their relative drift will continue to increase their spatial separation. In accordance with the analytical model, the relative drift is smaller for $\theta = \pi/4$ and smaller still for $\theta = 0$. When $\theta = 0$, the electrons and positrons have a slight drift in the opposite direction (negative x and positive x, respectively). This results from the difference in the Gouy phase of the first and second harmonic.

Figure 5 shows the corresponding transverse current densities for the cases displayed in Fig. 4. When $\theta = \pi/2$, the positive transverse drift of the electrons and the negative transverse drift of the positrons produce two lobes of current located symmetrically about the propagation axis. Near the propagation axis, the current density is nullified by the spatial overlap and near-equal drift of the charges. When $\theta = \pi/4$, the situation is similar, but the charges are more overlapped in space, resulting in a much smaller current density. When $\theta = 0$, the current density is barely distinguishable from noise.

The simulations presented in this section modeled the collision of zero-emittance electron beams with two-color laser pulses in 2D. Additional simulations were run to test the effect of emittance and dimensionality. A normalized emittance of 1 mm mrad, consistent with laser wakefield accelerators, had no observable effect on the results: the divergence resulting from the drift velocity was much greater than the divergence

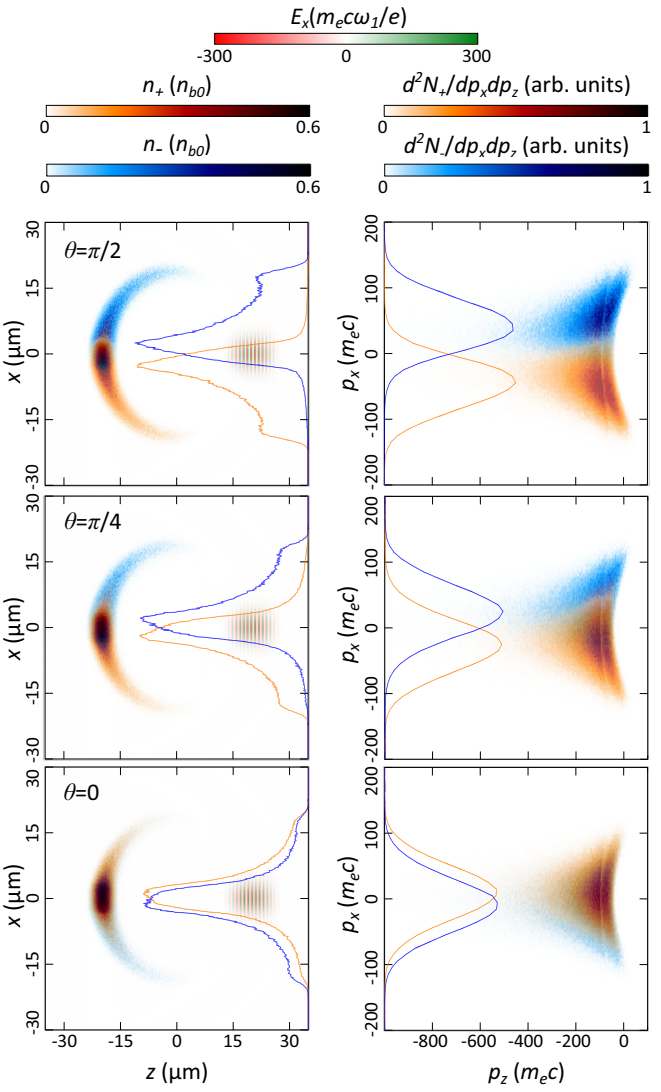

FIG. 4. Charge densities (left) and momentum distributions (right) of electrons (blue) and positrons (orange) created by the nonlinear Breit-Wheeler process ∼65 fs after the collision of a two-color laser pulse and relativistic electron beam. A phase offset of $\theta = \pi/2$ (top) between the first and second harmonic maximizes the spatial separation and relative drift of the electrons and positrons. The separation and relative drift are smaller for $\theta = \pi/4$ (middle) and are minimal for $\theta = 0$ (bottom). The line outs show the density and momentum distributions integrated over z and p_z, respectively.

of the incident electron beam. When the polarization of the two-color pulse was directed out of the plane, the pairs acquired transverse ($\hat{\mathbf{y}}$) momentum due to the ponderomotive force, but no net current was generated for any relative phase between the two colors. Thus, reasonable emittances and out-of-plane dynamics do not affect the principle result that an appropriately phased two-color laser pulse produces a net electron-positron current.

The two-color laser pulses used in the simulations had specified phase differences and transverse Gaussian profiles. In an experimental realization, the relative phase can be varied in a number of ways. For instance, in experiments where a two-color laser pulse generated a drift current of photonion-

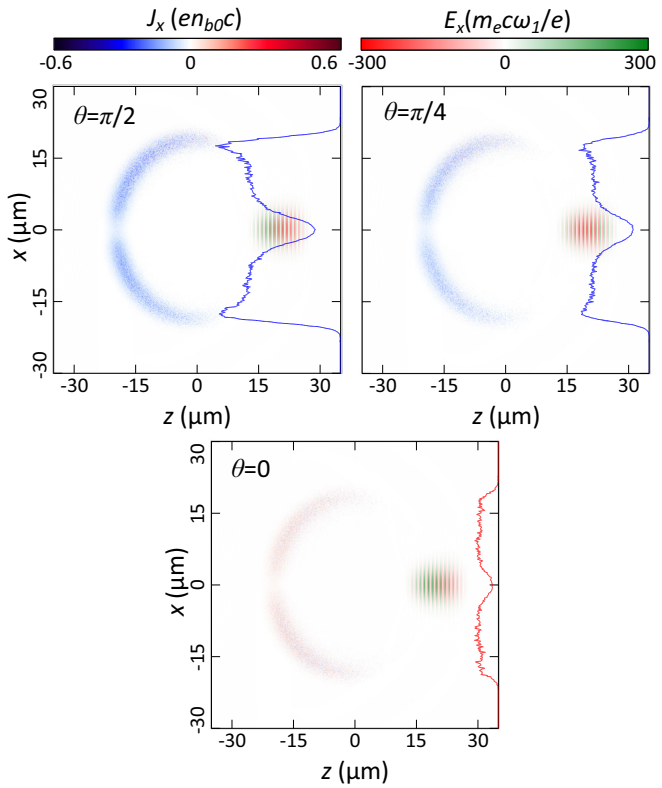

FIG. 5. Transverse current densities for the cases displayed in Fig. 4. The magnitude of the current density drops as the phase offset is decreased from $\theta = \pi/2$ to $\theta = 0$. The line outs show the integral of the current density over z. The large current density in the case of $\theta = \pi/2$ may provide a collective signature of nonlinear Breit-Wheeler pair creation.

ized electrons the relative phase was adjusted by shifting the longitudinal position of the frequency doubling crystal [56]. Ultimately, the ability to set the phase in a predictable way will depend on the shot-to-shot phase stability of the laser system. Regardless, Fig. 3(a) shows that there is a relatively wide range of phases around $\theta = \pi/2$ (or $3\pi/2$) where a large net current can be expected. As long as the two harmonics overlap in space and time, the production of a relative drift will not be sensitive to the spatial profile of the pulses: The transverse ponderomotive force results in a transverse velocity that is much smaller than the drift velocity.

IV. CONCLUSIONS AND PROSPECTS

A laser pulse composed of a fundamental and second harmonic provides control over the relative transverse motion of electrons and positrons created in the nonlinear Breit-Wheeler process. By adjusting the relative phase θ of the harmonics, the electrons and positrons can be made to drift in the opposite ($\theta = \pi/2$) or same direction ($\theta = 0$). In the case of $\theta = \pi/2$, the opposite drift spatially separates the charges, which can facilitate experimental detection and diagnosis of the pairs. The opposite drift also produces a transverse current density that can drive low-frequency radiation. This radiation may offer an additional diagnostic signature of nonlinear Breit-Wheeler. Finally, the asymptotic angle of the pairs $\sim p_{xf}/p_{zf}$ depends on the vector potential at the time of creation a_{x0}, which could provide an indirect measurement of its value [Eqs. (4) or (5)].

The underlying physics allowing for phase control was demonstrated using an analytical model and QED-PIC simulations with parameters motivated by near-term, high-power laser facilities and current laser wakefield accelerators. Second harmonic generation of a high-power (>5 PW) laser pulse has yet to be demonstrated and may be a technological challenge. Second (and third) harmonic generation of high-*energy* laser pulses is now routine at long-pulse facilities like OMEGA and NIF [82,83]. At a high-*power* laser facility featuring two laser pulses, such as the proposed EP-OPAL laser [77], a second harmonic conversion crystal could be placed before the final compression grating of one of the pulses. However, additional research is required to determine the feasibility of this approach. For example, the spectral acceptance of the frequency conversion crystal must accommodate the bandwidth of the short pulse, and high-efficiency compression gratings for ∼500 nm wavelengths would need to be fabricated.

This manuscript focused solely on the relative phase between two harmonics, but additional structuring of the optical waveform would allow for more exotic electron-positron motion. For instance, a two-color laser pulse with a time-dependent polarization could produce intertwined helical or twisted drifts. As another example, a two-color laser pulse with a higher-order transverse mode or orbital angular momentum could be used to spatially shape the drift motion and transverse current density. Finally, a two-color ultrashort flying focus [84–86] would provide control over the velocity of the pair-creation front, enabling a quasiparticle source of superradiant emission [87].

ACKNOWLEDGMENTS

The authors would like to thank Dr. Bertrand Martinez, Dr. Christophe Dorrer, and Óscar Amaro for many insightful and useful discussions. The authors acknowledge the support of the Fundação para a Ciência e a Tecnologia Grant No. PTDC/FIS-PLA/3800/2021 as well as PRACE for awarding access to MareNostrum based in the Barcelona Supercomputing Centre and LUMI based in the data center of CSC in Kajaani, Finland. The work of J.P.P., D.R., and K.W. is supported by the Office of Fusion Energy Sciences under Award No. DE-SC0021057, the Department of Energy National Nuclear Security Administration under Award No. DE-NA0003856, the University of Rochester, and the New York State Energy Research and Development Authority.

B.B. conducted and analyzed the OSIRIS simulations. The analytical model was developed by B.B., J.P.P., and M.V.. The manuscript was written by B.B. and J.P.P., with input from M.V., K.W., and D.R.. M.V. and J.P.P. supervised the project. All authors discussed the results presented in the paper.

APPENDIX: SIMULATION DETAILS

All simulations were run using the OSIRIS framework [64] with the Monte Carlo module for QED processes [66,69–73]. The "1D" simulations modeled a plane wave laser

pulse in a 2D domain with periodic boundary conditions in the transverse direction. The domain was 70 μm × 10 μm in the longitudinal (z) and transverse (x) directions, divided into 8600 × 320 cells. The asymptotic current density displayed in Fig. 3 was obtained by averaging over the x direction and summing over the z direction. The 2D simulations modeled a focused laser pulse with open boundary conditions. In this case, the domain was 70 μm × 60 μm, divided into 8640 × 1800 cells. Four particles per cell were used for the initial electron beam in the 2D simulations.

A 27 attosecond time step was used in all simulations, which ensured that the Courant-condition was satisfied and that in each time step the probabilities per particle for photon (NCS) and pair (nonlinear Breit-Wheeler) creation were much smaller than one. Thus, the probability that a single particle could be responsible for two creation events in a single time step was negligible.

The electric fields of the harmonics were initialized with the temporal profile $f(t) = 10(-|t| + \tau_s)^3/\tau_s^3 - 15(-|t| + \tau_s)^4/\tau_s^4 + 6(-|t| + \tau_s)^5/\tau_s^5$, where $\tau_s = 1.3\tau_{\mathrm{FWHM}} = 30$ fs. The value of $f(t)$ and its first two derivatives are zero at $|t| = \tau_s$, which provides smooth on and off ramps. This avoids the abrupt jumps that would occur with a Gaussian profile defined on a finite domain.

[1] P. Goldreich and W. H. Julian, Pulsar electrodynamics, Astrophys. J. **157**, 869 (1969).

[2] P. A. Sturrock, A model of pulsars, Astrophys. J. **164**, 529 (1971).

[3] M. A. Ruderman and P. G. Sutherland, Theory of pulsars: polar gaps, sparks, and coherent microwave radiation, Astrophys. J. **196**, 51 (1975).

[4] T. Damour and R. Ruffini, Quantum electrodynamical effects in Kerr-Newmann geometries, Phys. Rev. Lett. **35**, 463 (1975).

[5] G. W. Gibbons, Vacuum polarization and the spontaneous loss of charge by black holes, Commun. Math. Phys. **44**, 245 (1975).

[6] J. Arons and E. T. Scharlemann, Pair formation above pulsar polar caps: structure of the low altitude acceleration zone, Astrophys. J. **231**, 854 (1979).

[7] F. Takahara and M. Kusunose, Electron-positron pair production in a hot accretion plasma around a massive black hole, Prog. Theor. Phys. **73**, 1390 (1985).

[8] G. Henri and G. Pelletier, Relativistic electron-positron beam formation in the framework of the two-flow model for active galactic nuclei, Astrophys. J. **383**, L7 (1991).

[9] A. M. Beloborodov, Electron-positron outflows from gamma-ray emitting accretion discs, Mon. Not. R. Astron. Soc. **305**, 181 (1999).

[10] R. Ruffini, G. Vereshchagin, and S.-S. Xue, Electron–positron pairs in physics and astrophysics: From heavy nuclei to black holes, Phys. Rep. **487**, 1 (2010).

[11] F. Cruz, T. Grismayer, and L. O. Silva, Kinetic model of large-amplitude oscillations in neutron star pair cascades, Astrophys. J. **908**, 149 (2021).

[12] F. Cruz, T. Grismayer, A. Y. Chen, A. Spitkovsky, and L. O. Silva, Coherent emission from QED cascades in pulsar polar caps, Astrophys. J. Lett. **919**, L4 (2021).

[13] V. V. Uso, Millisecond pulsars with extremely strong magnetic fields as a cosmological source of γ-ray bursts, Nature (London) **357**, 472 (1992).

[14] P. Mészáros and M. J. Rees, Steep slopes and preferred breaks in gamma-ray burst spectra: The role of photospheres and comptonization, Astrophys. J. **530**, 292 (2000).

[15] M. H. P. M. van Putten, Electron-positron outflow from black holes, Phys. Rev. Lett. **84**, 3752 (2000).

[16] A. Pe'er and E. Waxman, Prompt gamma-ray burst spectra: Detailed calculations and the effect of pair production, Astrophys. J. **613**, 448 (2004).

[17] T. Siegert, R. Diehl, J. Greiner, M. G. H. Krause, A. M. Beloborodov, M. C. Bel, F. Guglielmetti, J. Rodriguez, A. W. Strong, and X. Zhang, Positron annihilation signatures associated with the outburst of the microquasar V404 Cygni, Nature (London) **531**, 341 (2016).

[18] E. S. Weibel, Spontaneously growing transverse waves in a plasma due to an anisotropic velocity distribution, Phys. Rev. Lett. **2**, 83 (1959).

[19] L. O. Silva, R. A. Fonseca, J. W. Tonge, J. M. Dawson, W. B. Mori, and M. V. Medvedev, Interpenetrating plasma shells: Near-equipartition magnetic field generation and nonthermal particle acceleration, Astrophys. J. **596**, L121 (2003).

[20] M. V. Medvedev, M. Fiore, R. A. Fonseca, L. O. Silva, and W. B. Mori, Long-time evolution of magnetic fields in relativistic gamma-ray burst shocks, Astrophys. J. **618**, L75 (2005).

[21] K. M. Schoeffler, N. F. Loureiro, R. A. Fonseca, and L. O. Silva, Magnetic-field generation and amplification in an expanding plasma, Phys. Rev. Lett. **112**, 175001 (2014).

[22] A. Schlüter, Über den ursprung der magnetfelder auf sternen und im interstellaren raum (Mit einem Anhang von A. Schlüter), Z. Naturforsch. A **5**, 65 (1950).

[23] J. Rafelski, L. P. Fulcher, and A. Klein, Fermions and bosons interacting with arbitrarily strong external fields, Phys. Rep. **38**, 227 (1978).

[24] A. Di Piazza, C. Müller, K. Z. Hatsagortsyan, and C. H. Keitel, Extremely high-intensity laser interactions with fundamental quantum systems, Rev. Mod. Phys. **84**, 1177 (2012).

[25] A. Gonoskov, T. G. Blackburn, M. Marklund, and S. S. Bulanov, Charged particle motion and radiation in strong electromagnetic fields, Rev. Mod. Phys. **94**, 045001 (2022).

[26] J. D. Brandenburg, J. Seger, Z. Xu, and W. Zha, Report on progress in physics: observation of the Breit–Wheeler process and vacuum birefringence in heavy-ion collisions, Rep. Prog. Phys. **86**, 083901 (2023).

[27] D. L. Burke, R. C. Field, G. Horton-Smith, J. E. Spencer, D. Walz, S. C. Berridge, W. M. Bugg, K. Shmakov, A. W. Weidemann, C. Bula *et al.*, Positron production in multiphoton light-by-light scattering, Phys. Rev. Lett. **79**, 1626 (1997).

[28] S. S. Bulanov, T. Z. Esirkepov, A. G. R. Thomas, J. K. Koga, and S. V. Bulanov, Schwinger limit attainability with extreme power lasers, Phys. Rev. Lett. **105**, 220407 (2010).

[29] H. Chen, S. C. Wilks, D. D. Meyerhofer, J. Bonlie, C. D. Chen, S. N. Chen, C. Courtois, L. Elberson, G. Gregori, W. Kruer *et al.*, Relativistic quasimonoenergetic positron jets from

intense laser-solid interactions, Phys. Rev. Lett. **105**, 015003 (2010).

[30] G. Sarri, K. Poder, J. M. Cole, W. Schumaker, A. Di Piazza, B. Reville, T. Dzelzainis, D. Doria, L. A. Gizzi, G. Grittani *et al.*, Generation of neutral and high-density electron–positron pair plasmas in the laboratory, Nat. Commun. **6**, 6747 (2015).

[31] M. Vranic, O. Klimo, G. Korn, and S. Weber, Multi-GeV electron-positron beam generation from laser-electron scattering, Sci. Rep. **8**, 4702 (2018).

[32] T. G. Blackburn and M. Marklund, Nonlinear Breit–Wheeler pair creation with bremsstrahlung γ rays, Plasma Phys. Control. Fusion **60**, 054009 (2018).

[33] A. Mercuri-Baron, M. Grech, F. Niel, A. Grassi, M. Lobet, A. D. Piazza, and C. Riconda, Impact of the laser spatio-temporal shape on Breit–Wheeler pair production, New J. Phys. **23**, 085006 (2021).

[34] A. Matheron, P. S. M. Claveria, R. Ariniello, H. Ekerfelt, F. Fiuza, S. Gessner, M. F. Gilljohann, M. J. Hogan, C. H. Keitel, A. Knetsch *et al.*, Probing strong-field QED in beam-plasma collisions, Commun. Phys. **6**, 141 (2023).

[35] H.-Y. Zhang, L.-F. Gan, H.-B. Zhuo, B. Qiao, Y.-Y. Ma, and J.-Y. Dai, Enhanced pair production in collisions of intense pulsed lasers with a high-energy electron beam, Phys. Rev. A **100**, 022122 (2019).

[36] J. Schwinger, On gauge invariance and vacuum polarization, Phys. Rev. **82**, 664 (1951).

[37] W. H. Furry, On bound states and scattering in positron theory, Phys. Rev. **81**, 115 (1951).

[38] H. Bethe and W. Heitler, On the stopping of fast particles and on the creation of positive electrons, Proc. R. Soc. London A **146**, 83 (1934).

[39] G. Breit and J. A. Wheeler, Collision of two light quanta, Phys. Rev. **46**, 1087 (1934).

[40] K. Sugimoto, Y. He, N. Iwata, I.-L. Yeh, K. Tangtartharakul, A. Arefiev, and Y. Sentoku, Positron generation and acceleration in a self-organized photon collider enabled by an ultraintense laser pulse, Phys. Rev. Lett. **131**, 065102 (2023).

[41] S. S. Bulanov, N. B. Narozhny, V. D. Mur, and V. S. Popov, Electron-positron pair production by electromagnetic pulses, J. Exp. Theor. Phys. **102**, 9 (2006).

[42] A. R. Bell and J. G. Kirk, Possibility of prolific pair production with high-power lasers, Phys. Rev. Lett. **101**, 200403 (2008).

[43] J. G. Kirk, A. R. Bell, and I. Arka, Pair production in counter-propagating laser beams, Plasma Phys. Control. Fusion **51**, 085008 (2009).

[44] S. S. Bulanov, V. D. Mur, N. B. Narozhny, J. Nees, and V. S. Popov, Multiple colliding electromagnetic pulses: A way to lower the threshold of e^+e^- pair production from vacuum, Phys. Rev. Lett. **104**, 220404 (2010).

[45] E. N. Nerush, I. Y. Kostyukov, A. M. Fedotov, N. B. Narozhny, N. V. Elkina, and H. Ruhl, Laser field absorption in self-generated electron-positron pair plasma, Phys. Rev. Lett. **106**, 035001 (2011).

[46] A. Zhidkov, S. Masuda, S. S. Bulanov, J. Koga, T. Hosokai, and R. Kodama, Radiation reaction effects in cascade scattering of intense, tightly focused laser pulses by relativistic electrons: Classical approach, Phys. Rev. ST Accel. Beams **17**, 054001 (2014).

[47] T. Grismayer, M. Vranic, J. L. Martins, R. A. Fonseca, and L. O. Silva, Laser absorption via quantum electrodynamics cascades in counter propagating laser pulses, Phys. Plasmas **23**, 056706 (2016).

[48] M. Vranic, T. Grismayer, R. A. Fonseca, and L. O. Silva, Electron–positron cascades in multiple-laser optical traps, Plasma Phys. Control. Fusion **59**, 014040 (2017).

[49] A. A. Mironov, A. M. Fedotov, and N. B. Narozhny, Generation of quantum-electrodynamic cascades in oblique collisions of ultrarelativistic electrons with an intense laser field, Quantum Electron. **46**, 305 (2016).

[50] M. Jirka, O. Klimo, S. V. Bulanov, T. Z. Esirkepov, E. Gelfer, S. S. Bulanov, S. Weber, and G. Korn, Electron dynamics and γ and e^-e^+ production by colliding laser pulses, Phys. Rev. E **93**, 023207 (2016).

[51] I. Y. Kostyukov and E. N. Nerush, Production and dynamics of positrons in ultrahigh intensity laser-foil interactions, Phys. Plasmas **23**, 093119 (2016).

[52] T. Grismayer, M. Vranic, J. L. Martins, R. A. Fonseca, and L. O. Silva, Seeded QED cascades in counterpropagating laser pulses, Phys. Rev. E **95**, 023210 (2017).

[53] M. Jirka, O. Klimo, M. Vranic, S. Weber, and G. Korn, QED cascade with 10 PW-class lasers, Sci. Rep. **7**, 15302 (2017).

[54] A. Ilderton, Trident pair production in strong laser pulses, Phys. Rev. Lett. **106**, 020404 (2011).

[55] M. J. Vrakking and S. Stolte, Coherent control of molecular orientation, Chem. Phys. Lett. **271**, 209 (1997).

[56] K. Y. Kim, J. H. Glownia, A. J. Taylor, and G. Rodriguez, Terahertz emission from ultrafast ionizing air in symmetry-broken laser fields, Opt. Express **15**, 4577 (2007).

[57] K. Y. Kim, A. J. Taylor, J. H. Glownia, and G. Rodriguez, Coherent control of terahertz supercontinuum generation in ultrafast laser–gas interaction, Nat. Photon. **2**, 605 (2008).

[58] M. Förster, T. Paschen, M. Krüger, C. Lemell, G. Wachter, F. Libisch, T. Madlener, J. Burgdörfer, and P. Hommelhoff, Two-color coherent control of femtosecond above-threshold photoemission from a tungsten nanotip, Phys. Rev. Lett. **117**, 217601 (2016).

[59] P. K. Maroju, M. Di Fraia, O. Plekan, M. Bonanomi, B. Merzuk, D. Busto, I. Makos, M. Schmoll, R. Shah, P. R. Ribič *et al.*, Attosecond coherent control of electronic wave packets in two-colour photoionization using a novel timing tool for seeded free-electron laser, Nat. Photon. **17**, 200 (2023).

[60] M. Tamburini, C. H. Keitel, and A. Di Piazza, Electron dynamics controlled via self-interaction, Phys. Rev. E **89**, 021201(R) (2014).

[61] Y.-Y. Chen, P.-L. He, R. Shaisultanov, K. Z. Hatsagortsyan, and C. H. Keitel, Polarized positron beams via intense two-color laser pulses, Phys. Rev. Lett. **123**, 174801 (2019).

[62] D. Seipt, D. Del Sorbo, C. P. Ridgers, and A. G. R. Thomas, Ultrafast polarization of an electron beam in an intense bichromatic laser field, Phys. Rev. A **100**, 061402(R) (2019).

[63] J. M. Dawson, Particle simulation of plasmas, Rev. Mod. Phys. **55**, 403 (1983).

[64] R. A. Fonseca, L. O. Silva, F. S. Tsung, V. K. Decyk, W. Lu, C. Ren, W. B. Mori, S. Deng, S. Lee, T. Katsouleas *et al.*, Osiris: A three-dimensional, fully relativistic particle in cell code for modeling plasma based accelerators, in *Computational Science — ICCS 2002*, edited by P. M. A. Sloot, A. G. Hoekstra, C. J. K. Tan, and J. J. Dongarra (Springer, Berlin, Heidelberg, 2002), pp. 342–351.

[65] M. Vranic, Extreme laser-matter interactions: multi-scale PIC modelling from the classical to the QED perspective, Ph.D. thesis, Universidade de Lisboa, Instituto Superior Técnico, Lisbon, 2015.

[66] M. Vranic, J. Martins, R. Fonseca, and L. Silva, Classical radiation reaction in particle-in-cell simulations, Comput. Phys. Commun. **204**, 141 (2016).

[67] L. Landau and E. Lifshitz, *The Classical Theory of Fields. Course of Theoretical Physics*, Course of Theoretical Physics, 4th ed. (Butterworth-Heinemann, Oxford, UK, 1980).

[68] A. D. Piazza, Exact solution of the Landau-Lifshitz equation in a plane wave, Lett. Math. Phys. **83**, 305 (2008).

[69] C. Ridgers, J. Kirk, R. Duclous, T. Blackburn, C. Brady, K. Bennett, T. Arber, and A. Bell, Modelling gamma-ray photon emission and pair production in high-intensity laser–matter interactions, J. Comput. Phys. **260**, 273 (2014).

[70] A. Gonoskov, S. Bastrakov, E. Efimenko, A. Ilderton, M. Marklund, I. Meyerov, A. Muraviev, A. Sergeev, I. Surmin, and E. Wallin, Extended particle-in-cell schemes for physics in ultrastrong laser fields: Review and developments, Phys. Rev. E **92**, 023305 (2015).

[71] A. I. Nikishov and V. I. Ritus, Pair production by a photon and photon emission by an electron in the field of ultra intense electromagnetic wave and in a constant field, J. Exptl. Theoret. Phys. (U.S.S.R.) **52**, 1707 (1967) [Sov. Phys. JETP **25**, 1135 (1967)].

[72] V. N. Baier and V. M. Katkov, Quantum effects in magnetic bremsstrahlung, Phys. Lett. A **25**, 492 (1967).

[73] N. P. Klepikov, Emission of photons or electron–positron pairs in magnetic fields, Zhur. Esptl. i Teoret. Fiz. **26**, 19 (1954).

[74] S. Weber, S. Bechet, S. Borneis, L. Brabec, M. Bučka, E. Chacon-Golcher, M. Ciappina, M. DeMarco, A. Fajstavr, K. Falk *et al.*, P3: An installation for high-energy density plasma physics and ultra-high intensity laser–matter interaction at Eli-Beamlines, Matter Radiat. Extrem. **2**, 149 (2017).

[75] D. Papadopoulos, J. Zou, C. Le Blanc, G. Chériaux, P. Georges, F. Druon, G. Mennerat, P. Ramirez, L. Martin, A. Fréneaux *et al.*, The Apollon 10 PW laser: experimental and theoretical investigation of the temporal characteristics, High Power Laser Sci. Eng. **4**, e34 (2016).

[76] J. W. Yoon, Y. G. Kim, I. W. Choi, J. H. Sung, H. W. Lee, S. K. Lee, and C. H. Nam, Realization of laser intensity over 10^{23} w/cm^2, Optica **8**, 630 (2021).

[77] J. Bromage, S.-W. Bahk, I. A. Begishev, C. Dorrer, M. J. Guardalben, B. N. Hoffman, J. B. Oliver, R. G. Roides, E. M. Schiesser, M. J. Shoup III *et al.*, Technology development for ultraintense all-OPCPA systems, High Power Laser Sci. Eng. **7**, e4 (2019).

[78] E. Esarey, C. B. Schroeder, and W. P. Leemans, Physics of laser-driven plasma-based electron accelerators, Rev. Mod. Phys. **81**, 1229 (2009).

[79] W. P. Leemans, A. J. Gonsalves, H.-S. Mao, K. Nakamura, C. Benedetti, C. B. Schroeder, C. Tóth, J. Daniels, D. E. Mittelberger, S. S. Bulanov, J.-L. Vay, C. G. R. Geddes, and E. Esarey, Multi-GeV electron beams from capillary-discharge-guided subpetawatt laser pulses in the self-trapping regime, Phys. Rev. Lett. **113**, 245002 (2014).

[80] A. J. Gonsalves, K. Nakamura, J. Daniels, C. Benedetti, C. Pieronek, T. C. H. de Raadt, S. Steinke, J. H. Bin, S. S. Bulanov, J. van Tilborg, C. G. R. Geddes, C. B. Schroeder, C. Tóth, E. Esarey, K. Swanson, L. Fan-Chiang, G. Bagdasarov, N. Bobrova, V. Gasilov, G. Korn, P. Sasorov, and W. P. Leemans, Petawatt laser guiding and electron beam acceleration to 8 GeV in a laser-heated capillary discharge waveguide, Phys. Rev. Lett. **122**, 084801 (2019).

[81] B. Miao, J. E. Shrock, L. Feder, R. C. Hollinger, J. Morrison, R. Nedbailo, A. Picksley, H. Song, S. Wang, J. J. Rocca, and H. M. Milchberg, Multi-GeV electron bunches from an all-optical laser wakefield accelerator, Phys. Rev. X **12**, 031038 (2022).

[82] T. R. Boehly, D. L. Brown, R. S. Craxton, R. L. Keck, J. P. Knauer, J. H. Kelly, T. J. Kessler, S. A. Kumpan, S. J. Loucks, S. A. Letzring *et al.*, Initial performance results of the OMEGA laser system, Opt. Commun. **133**, 495 (1997).

[83] P. J. Wegner, J. M. Auerbach, T. A. Biesiada, Jr., S. N. Dixit, J. K. Lawson, J. A. Menapace, T. G. Parham, D. W. Swift, P. K. Whitman, and W. H. Williams, NIF final optics system: frequency conversion and beam conditioning, in *Optical Engineering at the Lawrence Livermore National Laboratory II: The National Ignition Facility*, edited by M. A. Lane and C. R. Wuest, *International Society for Optics and Photonics* (SPIE, 2004), Vol. 5341, pp. 180–189.

[84] J. P. Palastro, J. L. Shaw, P. Franke, D. Ramsey, T. T. Simpson, and D. H. Froula, Dephasingless laser wakefield acceleration, Phys. Rev. Lett. **124**, 134802 (2020).

[85] M. V. Ambat, J. L. Shaw, J. J. Pigeon, K. G. Miller, T. T. Simpson, D. H. Froula, and J. P. Palastro, Programmable-trajectory ultrafast flying focus pulses, Opt. Express **31**, 31354 (2023).

[86] J. J. Pigeon, P. Franke, M. L. P. Chong, J. Katz, R. Boni, C. Dorrer, J. P. Palastro, and D. H. Froula, Interferometric measurements of the focal velocity and effective pulse duration of an ultrafast 'flying focus', in *CLEO 2023, Technical Digest Series held at Charlotte Convention Center, Charlotte, North Carolina, USA* (Optica Publishing Group, 2023).

[87] B. Malaca, M. Pardal, D. Ramsey, J. R. Pierce, K. Weichman, I. A. Andriyash, W. B. Mori, J. P. Palastro, R. A. Fonseca, and J. Vieira, Coherence and superradiance from a plasma-based quasiparticle accelerator, Nat. Photon. **18**, 39 (2024).